

ERVD: An Efficient and Robust ViT-Based Distillation Framework for Hash Remote Sensing Image Retrieval

Le Dong, Qixuan Cao, Lei Pu, Fangfang Wu, Weisheng Dong, *Member, IEEE*, Xin Li, *Fellow, IEEE*, Guangming Shi, *Fellow, IEEE*

Abstract—Existing Vision Transformer (ViT)-based methods for remote sensing images (RSIs) retrieval often suffer from significant limitations, particularly regarding the model efficiency. Knowledge distillation is employed to enable rapid and efficient information retrieval, however, most distillation approaches struggle to enable student networks to effectively acquire high-level abstract knowledge and semantic information. The lack of a holistic and hierarchical understanding of knowledge further hinders the improvement of retrieval performance. To address these issues, this paper proposes a novel ViT-based distillation framework, named ERVD. The framework introduces a high-level alignment module and a low-level alignment module to improve the student network’s capability to learn both holistic and detailed knowledge from the teacher network. Additionally, considering the challenges posed by small-scale remote sensing datasets and cluttered large-scene backgrounds, a novel plug-and-play data augmentation method is developed to enhance retrieval performance. Furthermore, the contrastive learning loss designed is integrated to minimize intra-class distances and maximize inter-class distances during iterative training. Extensive experiments on multiple datasets demonstrate the effectiveness and robustness of the proposed ERVD framework, showcasing superior performance compared to existing state-of-the-art methods. The code is available at <https://github.com/milkyfun0/ERVD>.

Index Terms—Image retrieval, vision transformer, knowledge distillation, data augmentation.

I. INTRODUCTION

WITH the rapid advancement of technology, a vast amount of remote sensing images (RSIs) has been generated, playing a crucial role in urban planning, environmental monitoring, and surveying [1]. Therefore, achieving efficient target image retrieval from massive RSIs has become an important challenge. As a result, RSIs retrieval methods have become a focal point of research, aiming at achieving faster and more cost-effective retrieval. Early remote sensing retrieval methods rely on manual annotation, where similar images are assigned identical and similar labels, enabling

retrieval through manual comparison [2]. However, manual annotation has become impractical for handling large-scale datasets with the explosion of RSIs, highlighting the urgent need for new retrieval approaches.

In recent years, hashing methods have gained widespread application in image retrieval due to their low computational and storage costs. Existing hashing methods can be broadly categorized into two types, including traditional hashing methods and deep learning-based hashing methods. Specifically, traditional hashing methods rely on hand-crafted image features, which are often invariant to transformations such as translation [3]. However, these hand-crafted features only capture certain aspects of the image and fail to accurately represent semantic information. This limitation reduces their performance and adaptability for specific retrieval tasks [4].

In contrast, deep neural networks have demonstrated powerful feature extraction capabilities for image retrieval, exemplified by models such as AlexNet [5], VGG [6], and ResNet [7]. In particular, all of these approaches are based on deep convolutional neural networks (CNN). In addition, the attention mechanism [8] has shown remarkable advantages in representation learning, leading to a series of Transformer-based methods that surpass traditional CNN approaches in various tasks such as image classification, object retrieval, and semantic extraction. Among these, the Vision Transformer (ViT) [9] divides input images into several 2D patches, projecting them into 1D vectors using a learnable linear projection matrix. Building upon the base ViT, researchers have proposed various ViT variants to enhance its performance in various vision tasks. While Transformer networks excel at capturing long-range dependencies, they often overlook local features. To address this limitation, methods such as Twins [10] and CAT [11] adopt an alternating local and global attention mechanism at different layers. The Swin Transformer [12] captures cross-window information by applying local attention within windows and implementing a shifted window partitioning strategy. The KVT model [13] introduces a KNN attention mechanism to further enhance model performance. Similar to CNNs, these innovations primarily aim to make ViT more adept at focusing on local image details. In addition to the above methods, other improvements include location coding [14] and standardized policies [15], which are aimed at further improving Transformer’s performance in visual tasks.

Unfortunately, while ViT effectively captures long-range dependencies in images, their computational cost is often sig-

Le Dong, Qixuan Cao, Weisheng Dong and Guangming Shi are with the School of Artificial Intelligence, Xidian University, Xi’an 710071, China. (e-mails: dongle@xidian.edu.cn; 3267928656@qq.com; wsdong@mail.xidian.edu.cn; gmshi@xidian.edu.cn).

Lei Pu is with the Combat Support College, Rocket Force Engineering University, Xi’an 710025, China. (e-mail: warmstoner@163.com)

Fangfang Wu is with the School of Computer Science and Technology, Xidian University, Xi’an 710071, China. (e-mail: wufangfang@xidian.edu.cn)

Xin Li is with the Dept. of Computer Science, University at Albany, Albany, NY 12222 USA. (e-mail: xli48@albany.edu) (*Corresponding author: Fangfang Wu*)

nificantly higher than that of CNNs, and their performance still lags behind CNNs in certain aspects [16]. This disparity is particularly pronounced in computationally constrained tasks like image retrieval, where ViTs' large computational overhead and parameter count limit their applicability. To enhance model efficiency, researchers have explored transferring knowledge from larger models to smaller ones. Hinton proposes the concept of knowledge distillation and defines three key parts of distillation, including knowledge, the distillation algorithm, and the teacher-student architecture [17], demonstrating the effectiveness of knowledge transfer. Subsequently, a series of knowledge distillation-based approaches have emerged. For instance, some studies leverage attention maps to represent knowledge for distillation [18], while others directly employ intermediate layers for hierarchical distillation [19], aiming to align the semantic information between the teacher and student models. However, these methods often fail to adequately perform hierarchical distillation from the perspectives of high-level abstract knowledge and low-dimensional semantic information. As a result, the student network only obtains the final output but lacks the essential preparatory knowledge required for comprehensive understanding.

Moreover, the aforementioned algorithms often rely on large datasets. Although they may perform well on training data, they frequently exhibit poor generalization on test data [20], a problem that becomes particularly pronounced when large-scale data are unavailable. As we all know, collecting and manually annotating datasets is typically expensive and time-consuming. Although natural image datasets such as ImageNet [21] are available, overfitting remains a significant challenge. To alleviate this issue, data augmentation techniques are commonly employed. These techniques can be broadly categorized into basic and advanced methods. Basic data augmentation includes techniques such as image cropping [22], flipping [23], adding noise [24], and interpolation [25]. Advanced data augmentation, on the other hand, focuses on image mixing and semantic-based methods, which often entail higher computational costs, particularly in remote sensing. Despite the emergence of new datasets, RSI datasets remain relatively scarce compared to those for natural images. Furthermore, efficient data augmentation methods tailored specifically for RSIs are still lacking.

To address the aforementioned challenges, an efficient and robust ViT-based distillation network architecture is proposed, for RSI retrieval, named ERVD, designed to make the network more streamlined and effective. Specifically, we develop a high-level module and a low-level alignment module to enhance the student network's ability to learn holistic and detailed knowledge. Specifically, the student network learn high-level semantic information from the teacher network in the high-level module. In the low-level alignment module, we incorporate global knowledge alignment and regional knowledge alignment, enabling the student network to better capture fine-grained knowledge. Furthermore, to mitigate the challenges posed by the small scale and cluttered backgrounds of RSIs, a novel data augmentation method is designed that effectively alleviates the impact of dataset limitations on retrieval performance. Finally, we introduce a supervised contrastive learning

approach, which constructs positive and negative samples based on labels and integrates a triplet loss function. This helps the model reduce intra-class distances and expand inter-class distances during iterative training. Compared to other state-of-the-art methods, our approach achieves superior performance across multiple datasets. To sum up, the contributions of this paper can be summarized as follows:

- 1) An efficient and robust RSIs retrieval method is proposed, featuring a ViT-based distillation network architecture. This design significantly reduces model parameters and computational costs while enhancing retrieval performance.
- 2) A novel hierarchical alignment method is designed, incorporating high-level alignment and low-level alignment modules, which enables the student network to learn high-level semantic information from the teacher network while effectively capturing fine-grained features, further enhancing retrieval performance.
- 3) A novel data augmentation method is introduced to address the challenges of small-scale datasets and cluttered backgrounds, which enhances the model's generalization ability and significantly improves performance across various datasets.
- 4) Experiments conducted on datasets such as UCMD, AID, and NWPU-RESISC45 demonstrate that our approach consistently achieves the highest MAP values across different bits, further validating the effectiveness and robustness.

The remainders of this paper are arranged as follows. Section II introduces some related works about the ViT and the Knowledge Distill. The designed network is showed in detail in Section III. The experimental results are discussed in Section IV. Section V presents the conclusions of our paper.

II. RELATED WORKS

A. Vision Transformer

The Transformer model [26] is initially proposed for sequential data and achieved remarkable success in the field of natural language processing (NLP). Inspired by its success in NLP, researchers begin exploring whether the Transformer architecture could similarly learn effective representations for image data in computer vision tasks. Specifically, ViT segments images into a series of patches and incorporates positional encoding to retain spatial information.

Subsequently, various ViT variants are developed for vision tasks with remarkable results, including enhanced locality [11] and architectural improvements [27]. Typically, ViT is pretrained on large-scale datasets and fine-tuned for smaller downstream tasks, where the prediction head is often replaced during fine-tuning. However, when trained on medium-sized datasets, ViT's performance can sometimes be suboptimal. In particular, with limited data, Transformers often struggle to fit the data effectively, avoiding overfitting but failing to generalize well [28]. Conversely, with sufficiently large-scale pretraining data, ViT demonstrates strong performance even on tasks involving smaller datasets.

Recently, the field of remote sensing has increasingly adopted ViT as replacements for CNNs to better extract semantic information from RSI. Compared to CNNs, ViTs excel at capturing long-range dependencies between regions. ViTs have been employed for semantic alignment in multimodal remote sensing retrieval. In [29], an interacting enhancing feature transformer has been developed to explore the deep connections between images and files, utilizing multimodal information to enhance visual features and improve retrieval performance. A transformer based encoder works on both text and vision, combining multiple languages in the encoder [30]. In addition, subaperture decomposition algorithm is used to enhance the performance of unsupervised learning retrieval in [31], which uses an unsupervised transformer autoencoder network. Han *et al.* propose a hash retrieval method based on focused attention features to solve the distribution problem of RSIs, which successfully alleviates the long-tail distribution problem [32]. HashFormer is also used to solve deep hash retrieval tasks, which greatly improves retrieval performance by using ViT as the backbone network and using binary code as the intermediate representation of data [33]. Unfortunately, these methods are very time and computationally expensive.

B. Knowledge Distillation

Systematic knowledge distillation, introduced by Hinton *et al.* [17], focuses on transferring knowledge from a teacher network to a student network through imitation. A major challenge is efficiently transferring knowledge from the teacher to the student model. The simplest method is for the student network to replicate the teacher network's final output, which is both straightforward and effective. Another approach involves having the student network progressively learn abstract features layer by layer, using process information as knowledge transfer to the student network, complementing the first method.

In [34], based on the CNN framework, the authors introduce a student network attention learning strategy to mimic the teacher network's attention, enhancing the performance of the student CNN network. Chen *et al.* propose a cross-layer knowledge distillation mechanism that automatically assigns adaptive target layers from the teacher network to the student network, enabling cross-layer supervision during training and demonstrating the semantic relationship between the teacher and student networks across different tasks [35]. Jiao *et al.* show a two-stage distillation method based on Transformer to introduce common knowledge from a large teacher network into the student model, greatly improving the speed of reasoning while maintaining accuracy [19]. In addition, given the high demand for simple and efficient network architectures in the remote sensing, knowledge distillation methods have also been widely applied in this field. Yang *et al.* propose a remote sensing semantic segmentation network based on knowledge distillation, and obtain a lightweight network model by training teacher-student models through model pruning and distillation frameworks [36]. And in [37], two distillation strategies and cross-modal weighted triplet losses are designed to monitor and ensure complete knowledge transfer, greatly improving retrieval efficiency.

C. Data Augmentation

Recently, data augmentation methods have played a crucial role in effectively addressing the problem of insufficient data in deep learning. Overall, these methods aim to solve two main issues. First, the problem of overfitting or the inability of the model to effectively fit the data due to data scarcity. Second, by providing the model with diverse image scenarios, they enhance the model's robustness. Common data augmentation techniques include simple yet effective methods such as image flipping, cropping, noise injection, color transformation, and image jittering [38].

More challenging methods involve randomly removing image regions during training. Kim *et al.* choose a limited set of local patches from the image and apply various augmentation strategies to each patch, generating diverse local augmentation samples for the network [39]. Zhong *et al.* propose a random erasure strategy to generate training images with different occlusion degrees, which extends the robustness of the CNN-based algorithms [40]. Similarly, chen *et al.* also propose a data augmentation algorithm based on random deletion to improve the diversity of data [24]. All these augmentation methods improve the model's understanding of data semantic information. Furthermore, to maintain task consistency, some researchers have proposed image mixing enhancement methods. For instance, Zhu *et al.* [41] propose directly mixing images at a certain ratio.

In the remote sensing field, where image data is relatively scarce, data augmentation methods are also frequently applied. For example, some studies have used data augmentation to create proxy tasks that help the model learn [42], while others have enhanced the model's understanding of scene semantics. In [43], image augmentation strategy is applied to low-quality images to improve the performance of remote sensing scene segmentation. In [44], multiple random initialization is used to consider multiple samples in semantic categories to enhance image retrieval performance. However, the complexity of these methods is high, which affects the application and performance of related algorithms.

III. PROPOSED METHOD

To realize more efficient and robust RSIs retrieval, we design a distillation network based on ViT in this paper, as is shown in Fig. 1. The model consists of five main components, including a teacher-student network, a hashing learning module, a distillation module, and a data augmentation module. Specifically, both the teacher and student networks are based on the ViT architecture, with their primary differences lying in the size of the hidden layers and the number of network layers. The student model autonomously learns representations through the hashing learning module. The distillation module facilitates the learning process by guiding the student network using both high-level and low-level information from the teacher network. Additionally, the data augmentation module is designed as a plug-and-play component to enhance the framework's flexibility.

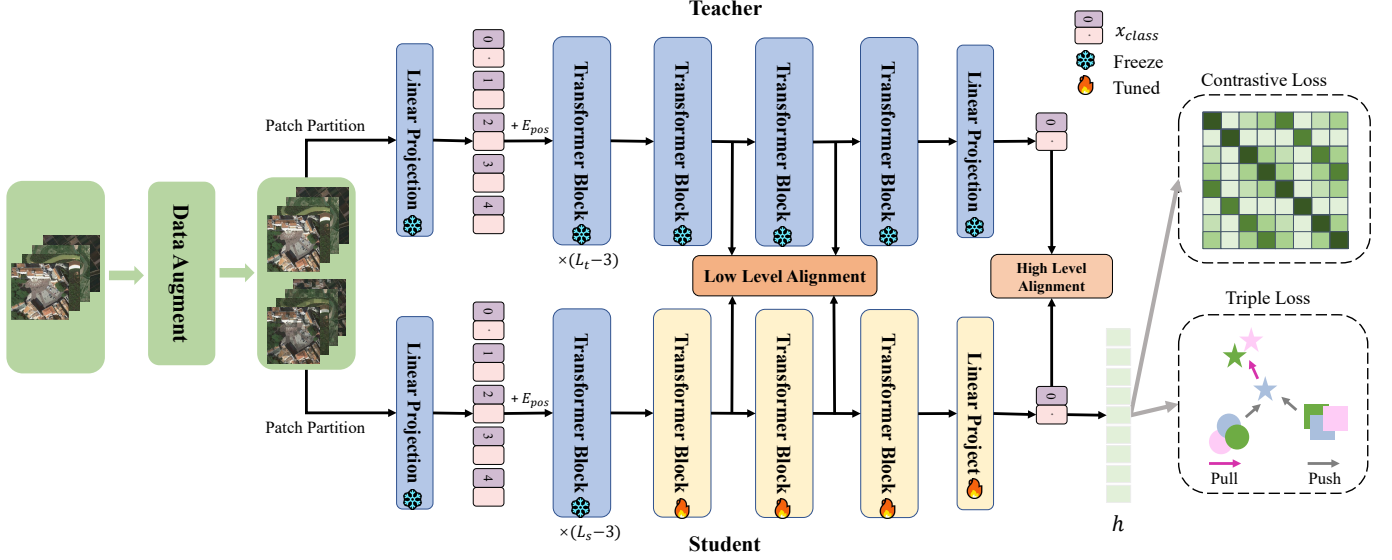


Fig. 1. Our proposed framework comprises four main components, including data augmentation Module, teacher-student framework, distillation module, and hashing learning. The distillation module is further divided into the high-level alignment Module and the low-level alignment module. The *Patch Partition* operation refers to dividing an image into several smaller patches, based on a specified patch size.

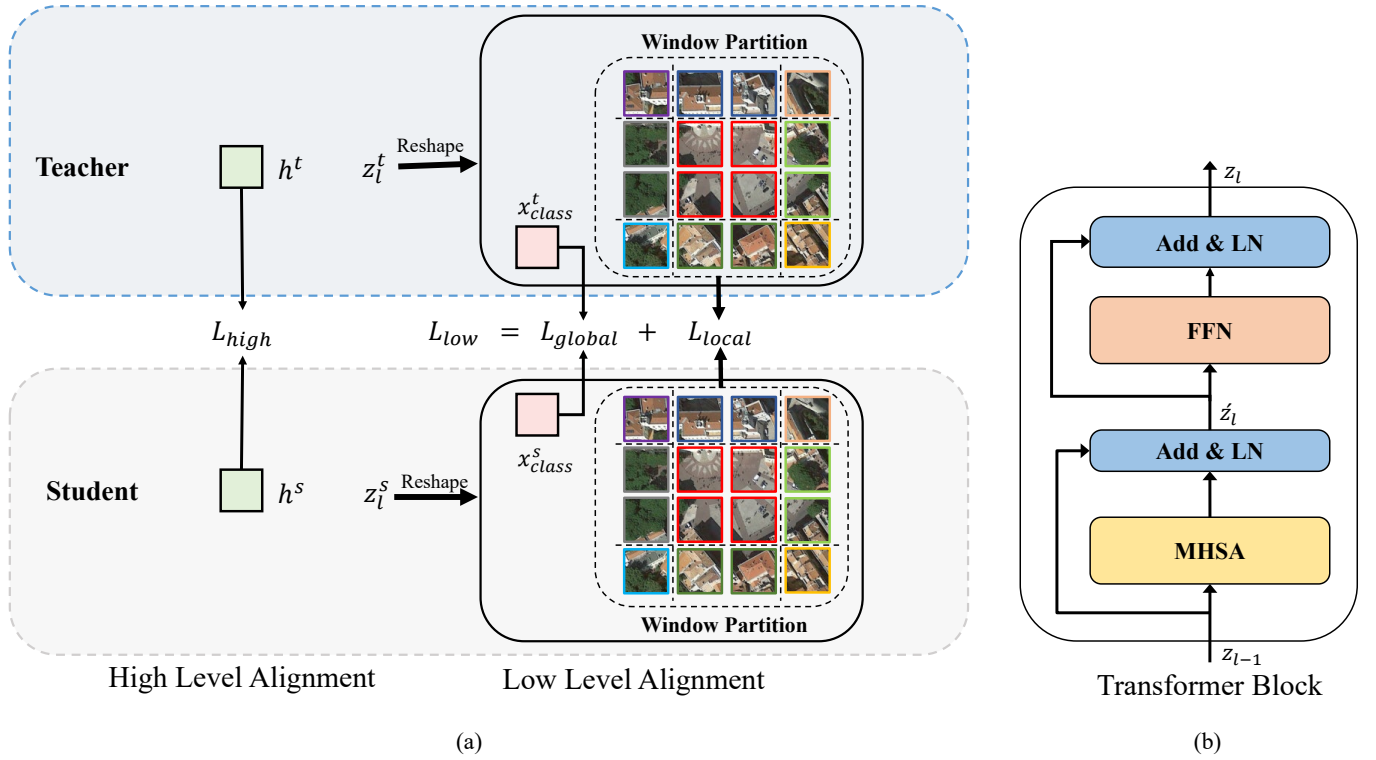


Fig. 2. (a) Distillation module. This module consists of the high-level alignment and low-level alignment sub-modules. Given that the hidden layers of the teacher network and the student network have different dimensions, a linear projection layer is employed to align their sizes. Notably, the weights of the linear layers used for alignment in the high-level and low-level alignment modules are not shared. (b) Transformer block diagram. The transformer block includes key components such as Multi-Head Self-Attention (MHSA) and Feed-Forward Network (FFN), supplemented by layer normalization and residual connections, to efficiently capture long-range dependencies and hierarchical feature representations.

A. Vision Transformer Framework

As is shown in Fig. 1, ViT replaces CNN as the foundational architecture. Notably, the classification layer of ViT is removed, while its core structure is retained to extract features from RSI. Specifically, assumed there are B training images $I = \{I_1, I_2, \dots, I_B\}$ and their corresponding labels $Y = \{y_1, y_2, \dots, y_B\}$, for any RSI $X \in I$, it is represented with three dimensions, including the number of channels C , height H , and width W . The image X is divided into patches of size $P \times P \times C$, resulting in N patches, where $N = \frac{H \times W}{P^2}$. These patches are denoted as $\{x_1, x_2, \dots, x_N\}$ with $x_i \in \mathbb{R}^{P^2 \times C}$. To capture global information, a learnable class token x_{class} is appended. Thus, the effective input sequence length for ViT is $N + 1$. At this stage, the initial input to the network z_0 can be defined as follows:

$$z_0 = [x_{class}; x_1E; x_2E; \dots; x_NE] + E_{pos} \quad (1)$$

where, $x_{class} \in \mathbb{R}^D$, $E \in \mathbb{R}^{(P^2C) \times D}$, $E_{pos} \in \mathbb{R}^{(N+1) \times D}$. D represents the dimension of the hidden layer in ViT, E is the embedding projection matrix for mapping patches into the hidden space, and E_{pos} denotes the learnable positional embedding matrix.

ViT consists of L Transformer blocks, as shown in Fig. 2(b). Each block contains multi-head self-attention layers and a fully connected layer. Add layer normalization before each layer and residual joins after it. The formula for Transformer Block is as follows:

$$\hat{z}_l = LN(MHSA(z_{l-1}) + z_{l-1}) \quad (2)$$

$$z_l = LN(FFN(\hat{z}_l) + \hat{z}_l) \quad (3)$$

where $l = 1, 2, \dots, L$. $MHSA$ and FFN represent the multi-head self-attention layer and the fully connected layer, respectively.

Teacher Network. The teacher network uses ViT as the basic model, and the parameters are set to $D_t = 512$ and $L_t = 12$. Since RSIs are different from natural images, more attention is paid to the extraction of local information. To improve the performance of teacher network, different from ViT-32, we set the patch size to $P_t = 16$ to improve the model's ability to control details.

Student Network. The structure of the student network is the same as that of the teacher network. To ensure the simplicity of the student network, the parameters are set to $D_s = 256$ and $L_s = 6$, thus significantly reducing the number of parameters and the amount of computation. Similarly, to enhance the ability of the model to capture details, the patch is also set to $P_s = 16$.

ViT Pre-trained Model. During retrieval, we use the pre-trained ViT to initialize the weights. Because of the particularity of hash retrieval task, the classification pre-training model trained on ImageNet is not used here, but the parameter weights of the pre-training model based on CLIP architecture are used [45], which can better extract the semantic information of images and distinguish different images. It is worth noting that we only use the pre-training parameter in the image encoder part to initialize the model. Previous research [46] shows that in the ViT framework, the model is better

at extracting local features in the first $\frac{L}{2}$ layer, while in the RSI retrieval task, it pays more attention to global feature learning. Therefore, during the training process, we freeze the parameters of the former $\frac{L}{2}$ layer of teacher network and student network, which not only reduces the difficulty of training, but also ensures the accuracy of the model.

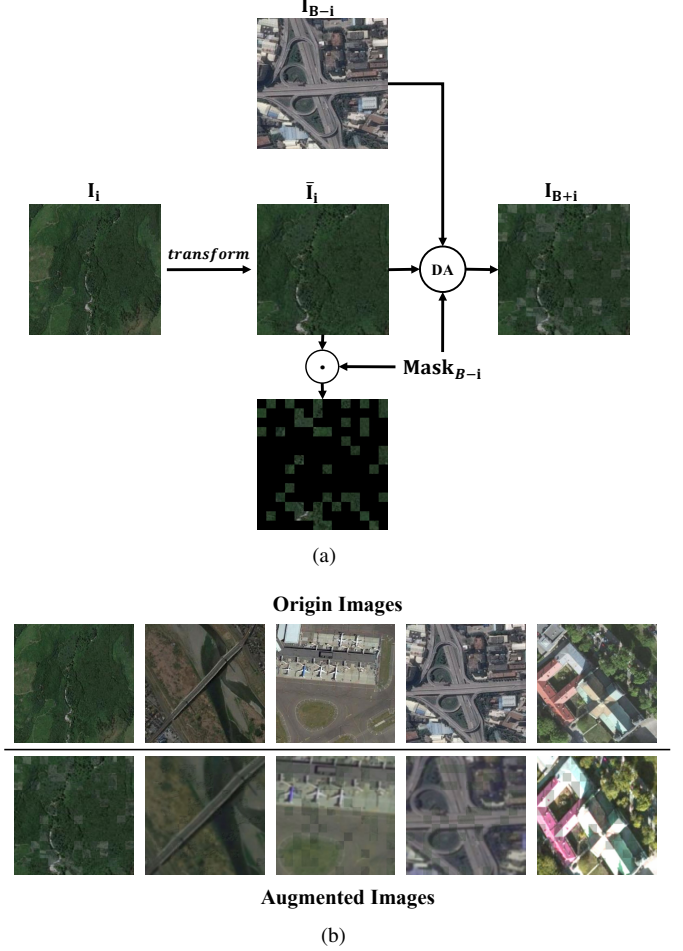


Fig. 3. (a) The data augmentation process. $transform$ represents the image transformation operations, the DA corresponds to Equation 11, \cdot denotes the dot product operation. I_{B+i} represents the augmented images. (b) Examples of images before and after data augmentation. Original Images represent the raw images, and Augmented Images are the transformed versions.

B. Knowledge Distill

As depicted in Fig. 2(a), the distillation module consists of a high-level alignment module and a low-level alignment module. The high-level alignment module primarily offers high-level knowledge guidance to the student network, assisting it in learning high-dimensional features. And the low level alignment module based on window partition enable the student network to pay attention to low dimensional information in images during training.

High Level Alignment Module. We take the hash feature h_t extracted by the teacher network as the soft label of the student network, and the loss function is defined as follows:

$$L_{high} = \|h^t - h^s\|_2 \quad (4)$$

where $h^t \in \mathbb{R}^b$ represents the hash features extracted by the teacher network, and $h^s \in \mathbb{R}^b$ is the hash features extracted by the student network.

Low Level Alignment Module. First, the output of the teacher network corresponding to any layer is $z^t \in \mathbb{R}^{(N+1) \times D}$, where $z^t = [x_{class}^t; x_1^t; x_2^t; \dots; x_N^t]$. Accordingly, the output of this layer of the student network is $z^s \in \mathbb{R}^{(N+1) \times D}$, where $z^s = [x_{class}^s; x_1^s; x_2^s; \dots; x_N^s]$. In particular, because the hidden layers of the teacher and student networks differ in size, they need to be mapped to the same dimensions using the full connection layer. Here, the loss function formula of the global feature alignment is as follows:

$$L_{global} = \|x_{class}^t W_1 - x_{class}^s\|_2 \quad (5)$$

where $W_1 \in \mathbb{R}^{D^t \times D^s}$, $x_{class}^t \in \mathbb{R}^{D^t}$, $x_{class}^s \in \mathbb{R}^{D^s}$.

Then, to better learn the image details, it is necessary to align the local features of the student network and the teacher network. Firstly, here we adjust the shape of $[x_1^t; x_2^t; \dots; x_N^t]$ to $X_{image}^t \in \mathbb{R}^{\lfloor \sqrt{N} \rfloor \times \lfloor \sqrt{N} \rfloor \times D^t}$. According to the Window Partition method in Swin Transformer [27], X_{image}^t is divided into K windows, and then the tokens in each window are evenly pooled to generate X_{win}^t . The formula can be expressed as follows:

$$wins^t = WP(X_{image}^t W_2, w) \quad (6)$$

$$X_{win}^t = [P(wins_1^t), \dots, P(wins_k^t)] \quad (7)$$

where WP is the Window Partition operation. $X_{win}^t \in \mathbb{R}^{K \times D^s}$, $W_2 \in \mathbb{R}^{D^t \times D^s}$, and $K = \left(\frac{\lfloor \sqrt{N} \rfloor}{w}\right)^2$, representing the total number of windows, with w as the window size. $wins^t$ is an array where each element contains a different number of tokens. $P(wins^t)$ indicates the average pooling of tokens. Then, do the same for $[x_1^s; x_2^s; \dots; x_N^s]$ and get $X_{win}^s \in \mathbb{R}^{K \times D^s}$.

Considering that the central region of RSI is often more significant, we assign different weights to each window. Specifically, the weight of each window is determined by the proportion of tokens it contains relative to the total number of tokens. This can be mathematically expressed as follows:

$$L_{local} = \sum_{i=1}^K p_i * \|X_{win_i}^s - X_{win_i}^t\|_2 \quad (8)$$

$$p_i = \frac{n(wins_i)}{N}, \quad i = 1, \dots, K \quad (9)$$

where $n(wins_i)$ represents the number of tokens within win_i . Finally, the loss function of the Low Level Alignment module is defined as:

$$L_{low} = L_{global} + L_{local} \quad (10)$$

C. Data Augmentation

Compared to natural images, the availability of RSI datasets are relatively limited, which can negatively impact model training performance. Although ViTs are less prone to overfitting on small datasets [28], the scarcity of RSI datasets combined with significant background noise presents unique

challenges. To address this problem, we propose a ViT-based data augmentation algorithm tailored for RSI. This algorithm features a plug-and-play data augmentation module, applied to image batches during training, while no augmentation is performed during testing.

As shown in Fig. 3, leveraging the characteristics of Transformers, we first apply random cropping, rotation, and color transformations to the RSIs. Next, a random masking operation is performed within patches to generate mask information. The processed images are then subjected to linear interpolation to produce the augmented images. The corresponding expression is as follows:

$$I_{B+i} = I_i + \lambda \cdot (\bar{I}_{B-i} - I_i) \odot \text{Mask}_{B-i} \quad (11)$$

$$\bar{I}_{B-i} = \text{transform}(I_{B-i}) \quad (12)$$

$$\text{Mask}_{B-i} = \mathcal{M}(I_{B-i}, p) \quad (13)$$

where $\lambda \in [0, 1]$ represents the image mixing ratio, while $p \in [0, 1]$ denotes the proportion of the image that is obscured. Both λ and p gradually increase as training progresses. The mask $\mathcal{M}_{B-i} \in \{0, 1\}^{H \times W}$ is a random binary matrix generated by the function $\mathcal{M}(I_{B-i}, p)$, and $\text{transform}()$ refers to a commonly used image transformation method.

The associated label of the augmented image remains unchanged:

$$y_{B+i} = y_i \quad (14)$$

Fig. 3 shows an example of before and after data augmentation images.

D. Hash Learning

To learn and generate hash coding, we further design a hash mapping layer to map class token z_L^0 to the corresponding hash feature. In the hash mapping layer, we use a two-layer multi-layer perceptron (MLP) structure to obtain the hash feature $h \in \mathbb{R}^b$, where b represents the hash bit of the hash code. The mathematical expression is as follows:

$$h = LN(z_L^0) W_1 W_2 \quad (15)$$

where LN stands for Layer Normalization, $W_1 \in \mathbb{R}^{D \times D}$, $W_2 \in \mathbb{R}^{D \times b}$. It is worth noting that the hash feature h is a continuous value during the training process and is only converted to a discrete value during the retrieval phase $\tilde{h} \in \{-1, 0, 1\}^b$. It can be expressed in the following formula:

$$\text{sign}(x) = \begin{cases} 1, & \text{if } x > 0 \\ 0, & \text{if } x = 0 \\ -1, & \text{if } x < 0 \end{cases} \quad (16)$$

$$\tilde{h} = \text{sign}(h). \quad (17)$$

E. Loss Function

Contrast learning loss function. In actual images, images with the same semantics may have significant visual differences, which can affect retrieval performance. To alleviate this issue, this paper introduces the InfoNCE loss, which can further improve retrieval capability by reducing intra class

spacing and increasing inter class gap. According to Huang *et al.* [47], the InfoNCE loss can be expressed as follows:

$$L_{info} = - \sum_{i \in P} \log \frac{\exp \left(h_i \cdot \frac{h_{j(i)}^T}{t} \right)}{\sum_{r \in R(i)} \exp \left(h_i \cdot \frac{h_r^T}{t} \right)} \quad (18)$$

where $P = \{1, \dots, 2B\}$ represents the index of the enhanced image. $R(i)$ represents the set P after removing i , and t is the temperature coefficient. In unsupervised learning, proxy tasks are typically used to generate positive sample pairs. Among them, h_i and $h_{j(i)}$ can be generated from the same image through different data augmentation methods. For positive sample h_i , there are usually $2B - 2$ negative samples.

Unlike unsupervised learning, there may be multiple positive samples due to the introduction of label information in supervised contrast learning. For h_i , the indexes with the same label are denoted as $S(i)$, and samples with different labels is denoted as a negative sample. In this case, there is no need to use a proxy task, so $P = \{1, 2, \dots, B\}$. In addition, since the original Softmax can cause numerical instability, we subtract a constant c from the sample similarity value set to the largest value in the vector. Hence, the new contrast loss in this paper can be expressed as:

$$L_{con} = \sum_{i \in P} \frac{-1}{n(S(i)) + \varepsilon} \sum_{s \in S(i)} \log \frac{\exp \left(\frac{(h_i \cdot h_s^T - c_i)}{t} \right)}{\sum_{r \in R(i)} \exp \left(\frac{(h_i \cdot h_r^T - c_i)}{t} \right)} \quad (19)$$

$$c_i = \max \{ h_i \cdot h_k^T \mid k \in R(i) \} \quad (20)$$

where $P = \{1, \dots, B\}$, $n(S(i))$ represents the number of samples in $S(i)$, and ε is a positive number used to prevent the denominator from being zero.

Triplet Loss function. To further reduce intra-class variance and enhance inter-class separability, we incorporate the Hamming distance-based triplet loss [48], which encourages samples within the same class to attract each other while pushing samples from different classes apart. The expression is given as:

$$L_{triple} = \frac{1}{B} \sum_{i=1}^B \sum_{j=1}^B l(h_i, h_j) \quad (21)$$

$$l(h_i, h_j) = \begin{cases} H(h_i, h_j) & \text{if } y_i = y_j \\ \max\{0, m - H(h_i, h_j)\} & \text{if } y_i \neq y_j \end{cases} \quad (22)$$

where $H(x, y)$ is the Hamming distance between x and y , and m is the margin.

Distillation loss function. The distillation loss function can be obtained from section III-B, expressed as follows:

$$L_d = \frac{1}{B} \sum_{i=1}^B (L_{high_i} + \gamma L_{low_i}) \quad (23)$$

$$L_{high_i} = \|h_i^t - h_i^s\|_2 \quad (24)$$

$$L_{low_i} = \sum_{m=1}^M (L_{global_i}^m + L_{local_i}^m) \quad (25)$$

where M indicates the number of Low Level Alignment modules, and γ indicates the hyperparameter.

Finally, the overall loss function of the proposed approach can be expressed as:

$$L^t = L_{con}^t + \alpha^t L_{triple}^t \quad (26)$$

$$L^s = L_{con}^s + \alpha^s L_{triple}^s + \beta^s L_d \quad (27)$$

where α^t , α^s and β^s are hyperparameters that adjust different loss ratios in training. L^t is the loss function for optimizing the teacher network, and L^s is for the student network.

IV. EXPERIMENTS

This section presents experiments to evaluate the effectiveness and robustness of the proposed framework. First, in Section IV-A, we describe three datasets used in the experiments. Then, the experimental details is described in Section IV-B. The experimental results are presented in Section IV-C, followed by a comparison of retrieval performance with different data augmentation methods in Section IV-E. Section IV-G verifies the effectiveness of our approach through ablation studies, and Section IV-D presents the parameter size and computational cost of different retrieval methods. Finally, the effectiveness of our method is discussed in Section IV-F.

A. Data Introduction

The University of California, Merced (UCMD) [57]. UCMD consists of 21 classes of RSIs, totaling 2100 images. Each class contains 100 images, with a resolution of 256×256 pixels and a spatial resolution of 0.3 meters.

The Aerial Image dataset (AID) [58]. AID contains 30 classes of RSIs, with a total of 10000 images. Each class includes between 220 and 420 images, with a resolution of 600×600 pixels and a spatial resolution ranging from 0.5 to 8 meters. Compared to UCMD, this dataset presents a greater retrieval challenge.

NWPU-RESISC45 Dataset [59]. NWPU-RESISC45 is a large-scale public dataset for the classification of remote sensing image scenes, containing 45 categories of remote sensing images, each containing 700 images with a resolution of 256×256 and a pixel resolution of 0.2 to 30 meters.

These three datasets have great differences in scene, scale and quantity, which provide strong support for the proposed method ERVD verification in this paper.

B. Experimental Details

In the experiments, as shown in Fig.1, both the teacher and student networks are based on the ViT architecture, with weights initialized from the image encoder of TinyCLIP [45], a model pretrained on the YFCC [60] dataset. For both the teacher and student networks, we train only the latter half, i.e., the $L/2$ Transformer Blocks. Importantly, since we freeze some layers of teacher network and student network, there are differences in the extraction of underlying semantic features between them. To this end, in the student network we only add the low level alignment module in the last two layers, with w set to 7, while the other unfrozen layers are used for

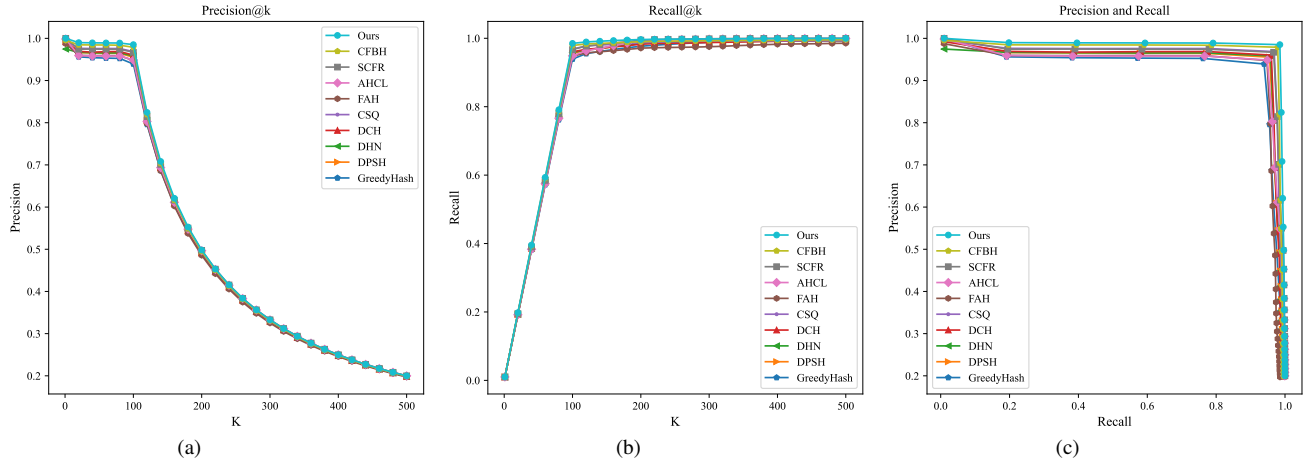


Fig. 4. Retrieval results on UCMD with 64-bit hash code. (a) Precision@k.(b) Recall@k (c) Precision and Recall.

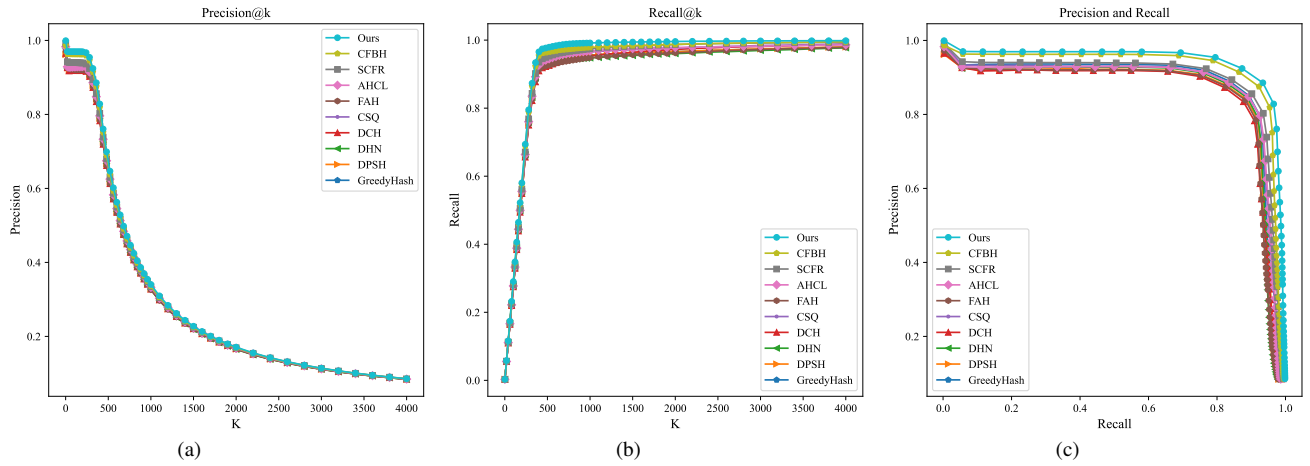


Fig. 5. Retrieval results on AID with 64-bit hash code. (a) Precision@k. (b) Recall@k (c) Precision and Recall.

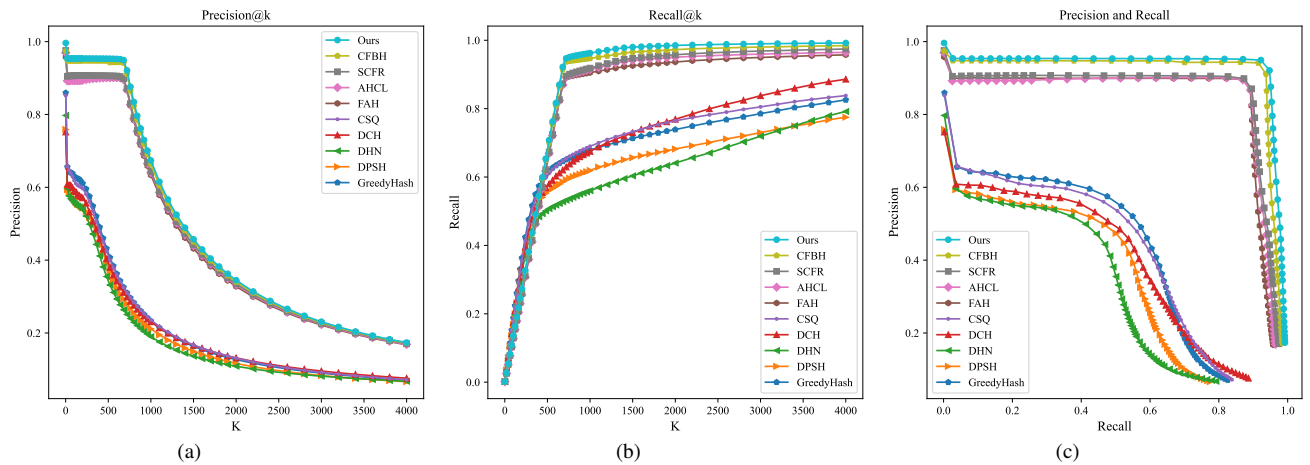


Fig. 6. Retrieval results on NWPU-RESISC45 with 64-bit hash code. (a) Precision@k. (b) Recall@k. (c) Precision and recall.

TABLE I
MAP RESULTS UNDER DIFFERENT BITS ON DIFFERENT DATASETS.

Methods	UCMD				AID				NWPU-RESISC45			
	32 bits	64 bits	128 bits	256 bits	32 bits	64 bits	128 bits	256 bits	32 bits	64 bits	128 bits	256 bits
Ours	98.37	99.03	98.55	98.96	96.40	97.19	97.38	97.63	94.83	95.62	95.95	96.48
CFBH [49]	97.89	98.48	98.51	98.87	95.27	96.32	96.12	96.51	94.06	94.88	94.69	94.93
SCFR [47]	97.65	97.95	98.29	98.14	93.79	94.42	94.59	94.53	90.48	91.11	91.78	91.79
FAH [50]	93.73	95.87	96.44	97.06	92.00	91.99	92.71	93.24	89.48	89.83	90.77	90.68
AHCL [51]	96.02	96.70	-	-	92.46	92.75	-	-	86.51	90.13	-	-
CSQ [52]	97.64	97.84	97.76	97.62	92.99	93.42	93.34	93.11	89.28	89.60	89.33	89.37
DCH [53]	97.27	97.13	96.20	95.79	91.91	91.71	91.27	91.14	88.78	87.99	87.63	87.17
GreedyHash [54]	96.16	95.60	97.05	93.28	92.39	93.24	93.73	94.18	89.53	90.59	90.83	91.19
DPSH [55]	94.02	96.92	97.27	97.21	92.09	92.25	92.45	92.24	67.50	88.85	88.01	85.62
DHN [56]	93.97	96.99	96.55	97.03	90.90	92.53	92.55	92.16	67.80	84.06	83.72	81.67

the self-adjustment of the student network to learn the bias information in the teacher network.

For each dataset, 70% of the images from each class are randomly chosen for training, and the remaining 30% are used for testing. All images are resized to 224×224 pixels before being input into the network. The network is trained using the SGD optimizer with a learning rate of 5×10^{-4} , a momentum of 0.9, and a weight decay of 1×10^{-4} . The mini-batch size is set to 128, and the temperature coefficient t is set to 0.1. The loss weight adjustment coefficients α^t , α^s , β^s and γ are set to 1, 2, 2, and 0.3, respectively. Additionally, The teacher network is trained for 100 epochs, while the student network is trained for 300 epochs. The experiments are performed using the Pytorch framework, with an Intel Xeon Gold 5218R CPU, dual NVIDIA GeForce RTX 2080Ti GPUs, and Python 3.9.

The Mean Average Precision (MAP), Precision@k, and Recall@k metrics are employed to assess retrieval performance. To validate the effectiveness of the proposed method, we evaluate it against nine state-of-the-art (SOTA) hashing retrieval methods, including three RSI retrieval methods, SCFR [47], FAH [50], and AHCL [51], as well as six natural image retrieval methods, CFBH [49], CSQ [52], DCH [53], DHN [56], DPSH [55], and GreedyHash [54].

TABLE II
COMPARISON OF METHODS ON UCMD, AID, AND NWPU-RESISC45 DATASETS

Methods	UCMD	AID	NWPU-RESISC45
MixUp [41]	98.00	96.79	95.82
CutMix [23]	98.17	96.65	95.08
GridMask [24]	98.01	96.75	95.65
PatchUp [25]	98.55	96.83	95.90
Ours	98.96	97.63	96.48

C. Retrieval Performance

To validate the effectiveness and robust of our method, we evaluate the performance of RSI retrieval using eight state-of-the-art (SOTA) hashing retrieval methods. Fig. 4, Fig. 5, and Fig. 6 illustrate the performance of different retrieval methods across various datasets. Table I shows the quantization results of all comparison methods and proposed method on three datasets of 32bits, 64bits, 128bits, and 256bits, respectively, where it can be seen from it that the proposed method has certain advanced nature.

On the UCMD dataset, as shown in Fig. 4, we compare the Precision@k, Recall@k, and Precision-Recall (PR) curves for various methods. Among the evaluated approaches, DHN, DPSH, and GreedyHash perform slightly worse on this dataset, while AHCL, FAH, and DCH achieve moderate results. SCFR and CFBH exhibit similar performance, both securing third place overall, while CFBH outperforms them, ranking second. Our method ERVD achieve a slight advantage over these approaches. As depicted in Fig. 4(b), the recall curves for all methods show minimal differences. However, in Fig.4(c), our method is clearly superior, with a PR curve that slightly outperforms those of other methods.

On the more challenging AID dataset, as shown in Fig. 5, we plot the Precision@k, Recall@k, and PR curves. The precision results, presented in Fig. 5(a), demonstrate that our method outperformed the others. Similarly, the recall curve in Fig. 5(b) indicates a slight advantage for our method. Notably, in the PR curve shown in Fig. 5(c), our retrieval performance is significantly better than that of the other methods.

On the most challenging NWPU-RESISC45 dataset, as illustrated in Fig. 6, we plot the same curves. From Fig. 6, it is evident that our method greatly outperform all others in terms of retrieval performance. Additionally, CFBH, SCFR, AHCL, and FAH achieve moderate results, ranking below our method. In contrast, CSQ, DCH, DHN, DPSH, and GreedyHash show poorer performance, as these methods are primarily designed for natural image retrieval.

In conclusion, our proposed method ERVD achieves superior performance compared to other nine approaches. In addition, the convergence results of the loss function during training with 128-bit hash codes are illustrated in Fig. 7. Across all three datasets, the loss function curves exhibit a consistent trend, that is, they decrease gradually and fluctuate within a small range, indicating steady convergence during training. On the AID and NWPU-RESISC45 datasets, the loss curves stabilize, and the model converge to a local optimum. However, on the UCMD dataset, the loss curve fluctuates more significantly than on the other datasets. This is likely due to the smaller size of the UCMD dataset, which leads to more pronounced adjustments in model weights and, consequently, greater oscillations in the loss curve.

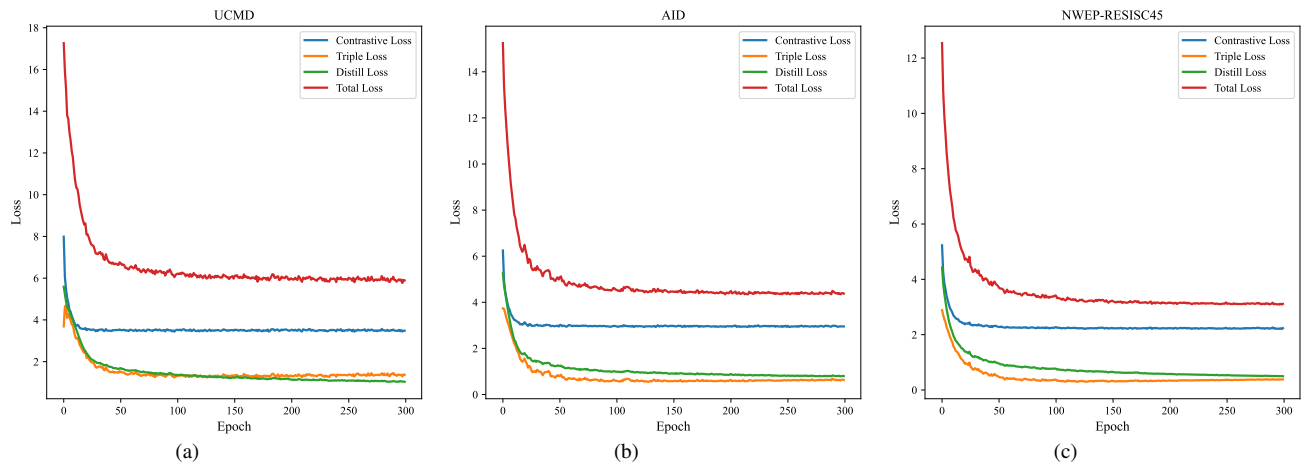


Fig. 7. Comparison of convergence results on different datasets. (a) UCMD. (b) AID. (c) NWP-RESISC45.

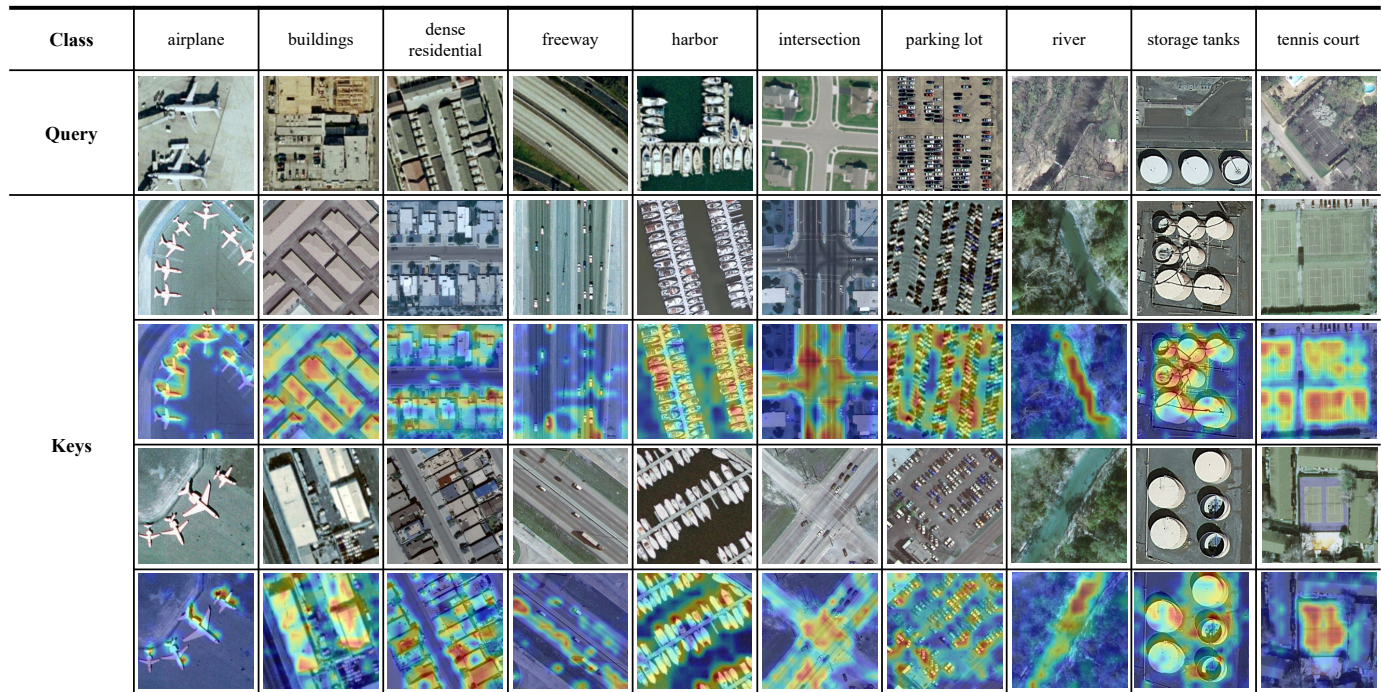


Fig. 8. The attention part of the retrieved image is visualized in heat map, and the red part represents the attention part of the model. Where Class represents the category, Query represents the Query Image, and Keys represents the similar image to be retrieved and its heat map.

TABLE III
ABLATION STUDY RESULTS ON DIFFERENT DATASETS.

Methods	UC Merced				AID				NWPU-RESISC45			
	32 bits	64 bits	128 bits	256 bits	32 bits	64 bits	128 bits	256 bits	32 bits	64 bits	128 bits	256 bits
Teacher	99.18	99.26	99.17	99.63	97.78	98.17	98.38	98.47	96.97	97.25	97.38	97.41
Method-1	92.83	93.78	95.79	95.21	91.91	93.05	93.93	93.83	89.39	90.85	91.25	91.77
Method-2	92.38	94.82	95.95	95.59	92.83	93.08	94.56	94.40	89.82	91.20	91.87	91.85
Method-3	97.55	98.02	98.13	98.19	94.26	95.91	96.37	96.59	92.41	94.39	95.04	95.18
Method-4	94.94	97.07	96.99	96.94	94.21	94.59	95.17	95.03	90.92	92.46	92.92	93.18
Method-5	96.43	97.27	97.45	97.11	94.60	95.22	95.49	95.62	91.56	92.67	93.14	93.36
Ours	98.37	99.03	98.55	98.96	96.40	97.19	97.38	97.63	94.83	95.62	95.95	96.48

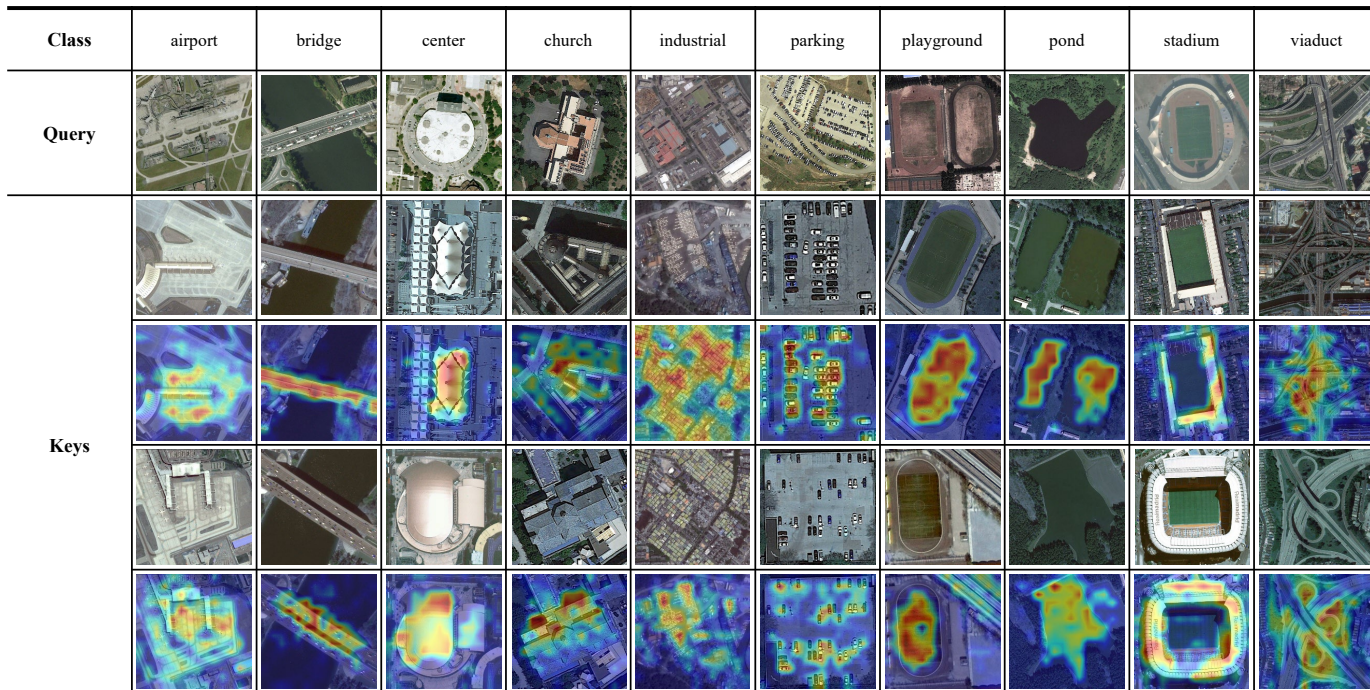


Fig. 9. On AID data set, the GradCam algorithm is used to visualize the heat map of the attention part of the retrieved Image during Query Image retrieval, and the red part represents the attention part of the model. Where Class represents the category, Query represents the Query Image, and Keys represents the similar image to be retrieved and its heat map.

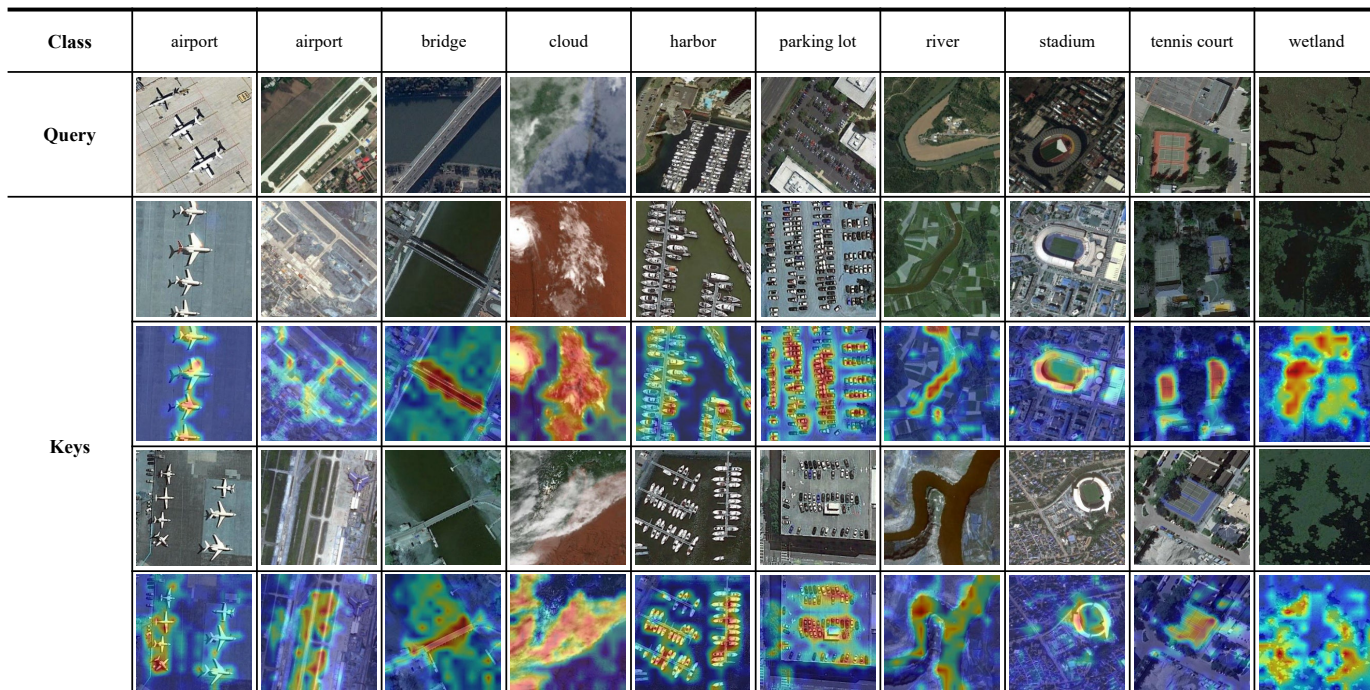


Fig. 10. On the NWPU-RESISC45 dataset, GradCam algorithm is used to visualize the heat map of the attention part of the retrieved Image during Query Image retrieval, and the red part represents the attention part of the model. Where Class represents the category, Query represents the Query Image, and Keys represents the similar image to be retrieved and its heat map.

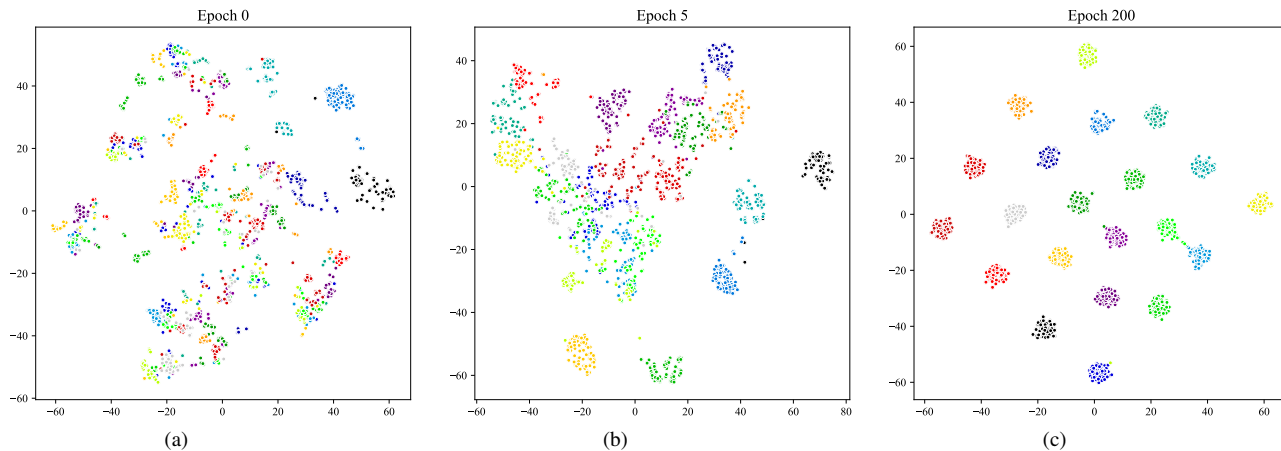


Fig. 11. On the UCMD dataset, the t-SNE algorithm [61] was used to project the high-dimensional space onto the 2-D plane and visualize the data distribution at different training stages. (a) Epoch 0. (b) Epoch 5. (c) Epoch 200.

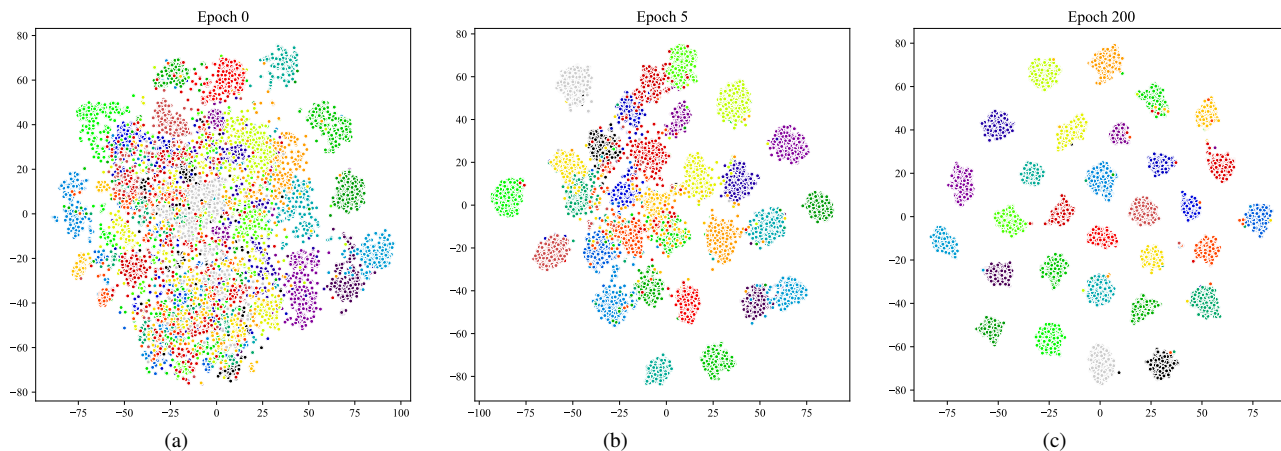


Fig. 12. On the AID dataset, the t-SNE algorithm is used to project the high-dimensional space to the 2-D plane, and the data distribution in different training stages is visualized. (a) Epoch 0. (b) Epoch 5. (c) Epoch 200.

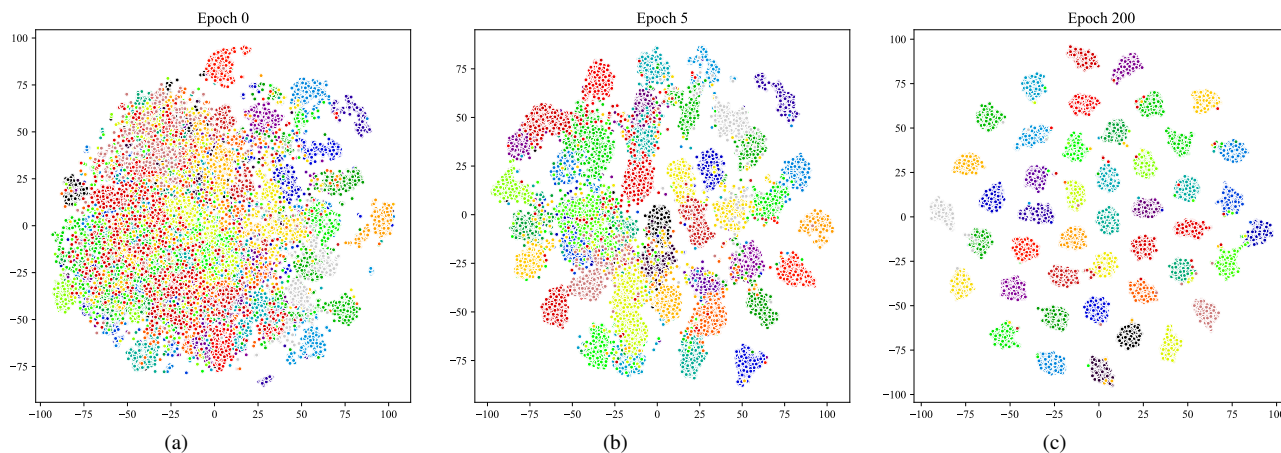


Fig. 13. On the NWPU-RESISC45 dataset, the t-SNE algorithm is used to project the high-dimensional space onto the 2D plane, and the data distribution in different training stages is visualized. (a) Epoch 0. (b) Epoch 5. (c) Epoch 200.

TABLE IV
COMPARISON OF TRAINING PARAMETERS AND FLOPS BETWEEN
DIFFERENT METHODS

	Teacher	Ours	CFBH	SCFR	FAH	CSQ	DCH	GreedyHash
Training	19.5M	2.5M	21.37M	58.1M	58.3M	239.2M	59.6M	134.8M
FLOPS	19.3G	0.65G	3.68G	0.71G	0.84G	6.5G	0.81G	15.4G

D. Efficiency Analysis

E. Data Augmentation Performance

In this subsection, we compare the performance of five different data augmentation methods across three datasets, including UCMD, AID, and NWPU-RESISC45, with 256-bit hash codes, as shown in Table. II. The results show that our method consistently outperformed others on all datasets. Specifically, our method achieve accuracy rates of 98.96%, 97.63%, and 96.48% on the UCMD, AID, and NWPU-RESISC45 datasets, respectively, significantly surpassing the performance of other methods. In contrast, the performance of the MixUp, CutMix, and GridMask methods show some fluctuations across the datasets. While MixUp perform well on UCMD and AID, its performance drop on NWPU-RESISC45. The PatchUp method show stable performance overall, with particularly strong results on UCMD and AID.

F. Model Analysis

When using hash codes for image retrieval, the goal is to ensure that images from the same category have minimal differences in their hash codes, while images from different categories exhibit significant differences. This subsection explores which parts of the query image the model focuses on during retrieval from the database. By leveraging the Grad-CAM method [62], the model’s attention is visualized using heatmaps. Fig. 8, Fig. 9 and Fig. 10 illustrate the visualization results across different datasets, where red indicates areas of high attention and blue denotes less significant regions.

As shown in Fig. 8, when the query image belongs to the airplane category, the model effectively identifies the key features of the airplane in the query image. Furthermore, it accurately locates the corresponding features and positions in the retrieved images, demonstrating the robustness of the proposed model. Additionally, our method exhibits a notable advantage in understanding fine-grained relationships within images. For instance, in the airport category shown in Fig. 9, the model first extracts semantic information about the airport from the query image. It then successfully identifies details such as airplanes and runways in the retrieved images, abstracting this fine-grained information into the airport category to complete the retrieval task. Finally, the model showcases high accuracy in regional recognition. For example, in the wetland category in Fig. 10, the model accurately identifies wetland regions in the retrieved images.

We utilize the t-SNE algorithm [61] to embed the hash codes generated from three datasets into a two-dimensional space for visualization, enabling us to observe their clustering performance at different training stages. As shown in Fig. 11, due to the smaller size of the UCMD dataset, our method

effectively separates different categories with ease. In Fig. 12, on the AID dataset, the proposed method achieves noticeable clustering even in the early stages of training. In Fig. 13, despite the challenges posed by the more complex NWPU-RESISC45 dataset, our approach demonstrates strong overall performance, with only a few samples showing anomalies. This is further evidenced in Fig. 13(c), where the clustering results highlight the method’s effectiveness. Lastly, as shown in Fig. 11(a), Fig. 12(a), and Fig. 13(a), certain categories exhibit clustering even without training the model, underscoring the effectiveness of the pre-trained parameters.

G. Ablation Study

In this section, we conduct a systematic ablation study to explore the impact of various components on the performance of our method. The study evaluates the effects of contrastive loss, triplet loss, high-level alignment loss (high-level loss), low-level alignment loss (low-level loss), and the data augmentation module. The ablation study includes five different configurations, as detailed below.

Method-1: Student + contrastive loss

Method-2: Student + contrastive loss + triplet loss

Method-3: Student + contrastive loss + triplet loss + data augment

Method-4: Student + contrastive loss + triplet loss + high level loss

Method-5: Student + contrastive loss + triplet loss + high level loss + low level loss

As mentioned earlier, the teacher network uses only contrast learning loss, triplet loss, and data enhancement, and freezes half of the network layer for training. And the student network also froze half of the network layer, and the training time is 300 epochs.

Method-1: This baseline model optimizes the student network using contrastive loss. While its performance on the UCMD dataset is slightly inferior to previous works, it demonstrates robustness on the more challenging AID and NWPU-RESISC45 datasets, highlighting the resilience of the student network.

Method-2: Building upon Method-1, this approach further constrains intra-class distances and enlarges inter-class distances. The results show overall improvement across all three datasets, with particularly notable gains on the AID dataset, while the enhancements on other datasets are less pronounced.

Method-3: By introducing a data augmentation module, this method achieves significant improvements across all datasets, validating the effectiveness of the proposed augmentation strategy.

Method-4: In this method, a teacher network is incorporated to guide the student network, building on Method-2. Compared to Method-2, this approach achieves noticeable performance gains across all datasets. The improvement can be attributed to the additional knowledge provided by the teacher network, which enhances the student network’s representational capacity and learning ability.

Method-5: Adding a hierarchical fine-grained alignment module allows the student network to learn detailed infor-

mation from the teacher network, further boosting the MAP scores.

Ours: Our final method combines the data augmentation module with Method-5, enhancing the model's robustness. As shown in the Table III, this approach achieves significant improvements across different datasets and hash bit lengths, demonstrating its effectiveness.

The training parameters and floating-point operations (FLOPs) require by different methods are summarized in Table IV. Compared to other methods and the teacher network, our method requires the least number of parameters and computations. Although the computational cost of the SCFR method is similar to ours, we achieve superior performance with fewer parameters. The smaller computational cost of other methods is primarily due to their use of CNN architectures, however, this also limits their ability to further reduce parameter size.

V. CONCLUSION

This paper proposes a Vision Transformer-based distillation framework for remote sensing image retrieval, integrating contrastive learning, triplet loss, and data augmentation to enhance retrieval performance. In addition, a novel data augmentation method is designed to solve the retrieval difficulties caused by large scale and complex background of environmental remote sensing scenes. Through ablation studies and efficiency analyses, we validate the effectiveness of the proposed method across multiple datasets, including UCMD, AID, and NWPU-RESISC45. Experimental results demonstrate that our approach outperforms existing methods in retrieval accuracy, precision, and robustness, making it an effective solution for large-scale, lightweight remote sensing image retrieval tasks.

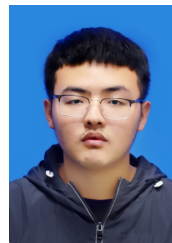
REFERENCES

- [1] L. Dong, Y. Yuan, and X. Luxs, "Spectral-spatial joint sparse nmf for hyperspectral unmixing," *IEEE Transactions on Geoscience and Remote Sensing*, vol. 59, no. 3, pp. 2391–2402, 2020. 1
- [2] W. Xiong, Z. Xiong, Y. Cui, L. Huang, and R. Yang, "An interpretable fusion siamese network for multi-modality remote sensing ship image retrieval," *IEEE Trans. Circuits Syst. Video Technol.*, vol. 33, no. 6, pp. 2696–2712, 2023. 1
- [3] D. G. Lowe, "Distinctive image features from scale-invariant keypoints," *International journal of computer vision*, vol. 60, pp. 91–110, 2004. 1
- [4] M. Datar, N. Immorlica, P. Indyk, and V. S. Mirrokni, "Locality-sensitive hashing scheme based on p-stable distributions," in *Proceedings of the twentieth annual symposium on Computational geometry*, 2004, pp. 253–262. 1
- [5] A. Krizhevsky, I. Sutskever, and G. E. Hinton, "Imagenet classification with deep convolutional neural networks," *Advances in neural information processing systems*, vol. 25, 2012. 1
- [6] K. Simonyan and A. Zisserman, "Very deep convolutional networks for large-scale image recognition," *arXiv preprint arXiv:1409.1556*, 2014. 1
- [7] K. He, X. Zhang, S. Ren, and J. Sun, "Deep residual learning for image recognition," in *Proceedings of the IEEE conference on computer vision and pattern recognition*, 2016, pp. 770–778. 1
- [8] S. Li, X. Xu, X. Jiang, F. Shen, X. Liu, and H. T. Shen, "Multi-grained attention network with mutual exclusion for composed query-based image retrieval," *IEEE Trans. Circuits Syst. Video Technol.*, vol. 34, no. 4, pp. 2959–2972, 2024. 1
- [9] C. Guo, K. Liu, D. Deng, and X. Li, "Vit spatio-temporal feature fusion for aerial object tracking," *IEEE Trans. Circuits Syst. Video Technol.*, vol. 34, no. 8, pp. 6749–6761, 2024. 1
- [10] X. Chu, Z. Tian, Y. Wang, B. Zhang, H. Ren, X. Wei, H. Xia, and C. Shen, "Twins: Revisiting the design of spatial attention in vision transformers," *Advances in neural information processing systems*, vol. 34, pp. 9355–9366, 2021. 1
- [11] H. Lin, X. Cheng, X. Wu, and D. Shen, "Cat: Cross attention in vision transformer," in *2022 IEEE international conference on multimedia and expo (ICME)*. IEEE, 2022, pp. 1–6. 1, 2
- [12] L. Qin, M. Wang, C. Deng, K. Wang, X. Chen, J. Hu, and W. Deng, "Swinface: A multi-task transformer for face recognition, expression recognition, age estimation and attribute estimation," *IEEE Trans. Circuits Syst. Video Technol.*, vol. 34, no. 4, pp. 2223–2234, 2024. 1
- [13] P. Wang, X. Wang, F. Wang, M. Lin, S. Chang, H. Li, and R. Jin, "Kvt: k-nn attention for boosting vision transformers," in *European conference on computer vision*. Springer, 2022, pp. 285–302. 1
- [14] X. Chu, Z. Tian, B. Zhang, X. Wang, and C. Shen, "Conditional positional encodings for vision transformers," *arXiv preprint arXiv:2102.10882*, 2021. 1
- [15] K. Wu, H. Peng, M. Chen, J. Fu, and H. Chao, "Rethinking and improving relative position encoding for vision transformer," in *Proceedings of the IEEE/CVF International Conference on Computer Vision*, 2021, pp. 10 033–10 041. 1
- [16] Y. Liu, Y. Zhang, Y. Wang, F. Hou, J. Yuan, J. Tian, Y. Zhang, Z. Shi, J. Fan, and Z. He, "A survey of visual transformers," *IEEE Transactions on Neural Networks and Learning Systems*, 2023. 2
- [17] G. Hinton, O. Vinyals, and J. Dean, "Distilling the knowledge in a neural network," *arXiv preprint arXiv:1503.02531*, 2015. 2, 3
- [18] Y. Dai, Y. Li, D. Chen, J. Li, and G. Lu, "Multimodal decoupled distillation graph neural network for emotion recognition in conversation," *IEEE Trans. Circuits Syst. Video Technol.*, vol. 34, no. 10, pp. 9910–9924, 2024. 2
- [19] X. Jiao, Y. Yin, L. Shang, X. Jiang, X. Chen, L. Li, F. Wang, and Q. Liu, "Tinybert: Distilling bert for natural language understanding," *arXiv preprint arXiv:1909.10351*, 2019. 2, 3
- [20] T. Kumar, A. Mileo, R. Brennan, and M. Bendechache, "Image data augmentation approaches: A comprehensive survey and future directions," *arXiv preprint arXiv:2301.02830*, 2023. 2
- [21] J. Deng, W. Dong, R. Socher, L.-J. Li, K. Li, and L. Fei-Fei, "Imagenet: A large-scale hierarchical image database," in *2009 IEEE conference on computer vision and pattern recognition*. Ieee, 2009, pp. 248–255. 2
- [22] H. Qin, H. Xi, Y. Li, M. A. El-Yacoubi, J. Wang, and X. Gao, "Adversarial learning-based data augmentation for palm-vein identification," *IEEE Trans. Circuits Syst. Video Technol.*, vol. 34, no. 6, pp. 4325–4341, 2024. 2
- [23] S. Yun, D. Han, S. J. Oh, S. Chun, J. Choe, and Y. Yoo, "Cutmix: Regularization strategy to train strong classifiers with localizable features," in *Proceedings of the IEEE/CVF international conference on computer vision*, 2019, pp. 6023–6032. 2, 9
- [24] P. Chen, S. Liu, H. Zhao, and J. Jia, "Gridmask data augmentation," *arXiv preprint arXiv:2001.04086*, 2020. 2, 3, 9
- [25] M. Faramarzi, M. Amini, A. Badrinarayanan, V. Verma, and S. Chandar, "Patchup: A feature-space block-level regularization technique for convolutional neural networks," in *Proceedings of the AAAI Conference on Artificial Intelligence*, vol. 36, no. 1, 2022, pp. 589–597. 2, 9
- [26] A. Vaswani, N. Shazeer, N. Parmar, J. Uszkoreit, L. Jones, A. N. Gomez, Ł. Kaiser, and I. Polosukhin, "Attention is all you need," *Advances in neural information processing systems*, vol. 30, 2017. 2
- [27] Z. Liu, Y. Lin, Y. Cao, H. Hu, Y. Wei, Z. Zhang, S. Lin, and B. Guo, "Swin transformer: Hierarchical vision transformer using shifted windows," in *Proceedings of the IEEE/CVF international conference on computer vision*, 2021, pp. 10 012–10 022. 2, 6
- [28] N. Park and S. Kim, "How do vision transformers work?" *arXiv preprint arXiv:2202.06709*, 2022. 2, 6
- [29] X. Tang, Y. Wang, J. Ma, X. Zhang, F. Liu, and L. Jiao, "Interacting-enhancing feature transformer for cross-modal remote sensing image and text retrieval," *IEEE Transactions on Geoscience and Remote Sensing*, 2023. 3
- [30] N. A. Alsharif, Y. Bazi, and M. M. Al Rahhal, "Remote sensing image retrieval using multilingual texts," in *IGARSS 2022 - 2022 IEEE International Geoscience and Remote Sensing Symposium*, 2022, pp. 1520–1523. 3
- [31] N.-C. Ristea, A. Anghel, M. Datcu, and B. Chapron, "Guided unsupervised learning by subaperture decomposition for ocean sar image retrieval," *IEEE Transactions on Geoscience and Remote Sensing*, 2023. 3
- [32] L. Han, M. E. Paoletti, S. Moreno-Álvarez, J. M. Haut, R. Pastor-Vargas, and A. Plaza, "Hashing for retrieving long-tailed distributed remote sensing images," *IEEE Transactions on Geoscience and Remote Sensing*, 2024. 3
- [33] T. Li, Z. Zhang, L. Pei, and Y. Gan, "Hashformer: Vision transformer based deep hashing for image retrieval," *IEEE Signal Processing Letters*, vol. 29, pp. 827–831, 2022. 3

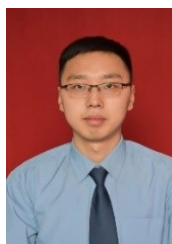
- [34] S. Zagoruyko and N. Komodakis, "Paying more attention to attention: Improving the performance of convolutional neural networks via attention transfer," *arXiv preprint arXiv:1612.03928*, 2016. 3
- [35] D. Chen, J.-P. Mei, Y. Zhang, C. Wang, Z. Wang, Y. Feng, and C. Chen, "Cross-layer distillation with semantic calibration," in *Proceedings of the AAAI conference on artificial intelligence*, vol. 35, no. 8, 2021, pp. 7028–7036. 3
- [36] Y. Yang, Y. Wang, J. Dong, and B. Yu, "A knowledge distillation-based ground feature classification network with multiscale feature fusion in remote sensing images," *IEEE Journal of Selected Topics in Applied Earth Observations and Remote Sensing*, 2023. 3
- [37] J. Guo, X. Guan, Y. Liu, and Y. Lu, "Distillation-based hashing transformer for cross-modal vessel image retrieval," *IEEE Geoscience and Remote Sensing Letters*, 2023. 3
- [38] T. Chen, S. Kornblith, M. Norouzi, and G. Hinton, "A simple framework for contrastive learning of visual representations," in *International conference on machine learning*. PMLR, 2020, pp. 1597–1607. 3
- [39] Y. Kim, A. S. Uddin, and S.-H. Bae, "Local augment: Utilizing local bias property of convolutional neural networks for data augmentation," *IEEE Access*, vol. 9, pp. 15 191–15 199, 2021. 3
- [40] Z. Zhong, L. Zheng, G. Kang, S. Li, and Y. Yang, "Random erasing data augmentation," in *Proceedings of the AAAIchen2020gridmask conference on artificial intelligence*, vol. 34, no. 07, 2020, pp. 13 001–13 008. 3
- [41] H. Zhang, M. Cisse, Y. N. Dauphin, and D. Lopez-Paz, "mixup: Beyond empirical risk minimization," *arXiv preprint arXiv:1710.09412*, 2017. 3, 9
- [42] Z. Yuan, W. Zhang, X. Rong, X. Li, J. Chen, H. Wang, K. Fu, and X. Sun, "A lightweight multi-scale crossmodal text-image retrieval method in remote sensing," *IEEE Transactions on Geoscience and Remote Sensing*, vol. 60, pp. 1–19, 2021. 3
- [43] C. Chen and L. Fan, "Scene segmentation of remotely sensed images with data augmentation using u-net++," in *2021 International Conference on Computer Engineering and Artificial Intelligence (ICCEAI)*. IEEE, 2021, pp. 201–205. 3
- [44] Y. Li, M. Hao, R. Liu, Z. Zhang, H. Zhu, and Y. Zhang, "Semantic-aware attack and defense on deep hashing networks for remote-sensing image retrieval," *IEEE Transactions on Geoscience and Remote Sensing*, vol. 61, pp. 1–14, 2023. 3
- [45] K. Wu, H. Peng, Z. Zhou, B. Xiao, M. Liu, L. Yuan, H. Xuan, M. Valenzuela, X. S. Chen, X. Wang *et al.*, "Tinyclip: Clip distillation via affinity mimicking and weight inheritance," in *Proceedings of the IEEE/CVF International Conference on Computer Vision*, 2023, pp. 21 970–21 980. 5, 7
- [46] S. Wang, J. Gao, Z. Li, X. Zhang, and W. Hu, "A closer look at self-supervised lightweight vision transformers," in *International Conference on Machine Learning*. PMLR, 2023, pp. 35 624–35 641. 5
- [47] M. Huang, L. Dong, W. Dong, and G. Shi, "Supervised contrastive learning based on fusion of global and local features for remote sensing image retrieval," *IEEE Transactions on Geoscience and Remote Sensing*, 2023. 7, 9
- [48] F. Schroff, D. Kalenichenko, and J. Philbin, "Facenet: A unified embedding for face recognition and clustering," in *Proceedings of the IEEE conference on computer vision and pattern recognition*, 2015, pp. 815–823. 7
- [49] X. Xiang, X. Ding, L. Jin, Z. Li, J. Tang, and R. Jain, "Alleviating over-fitting in hashing-based fine-grained image retrieval: From causal feature learning to binary-injected hash learning," *IEEE Transactions on Multimedia*, 2024. 9
- [50] C. Liu, J. Ma, X. Tang, F. Liu, X. Zhang, and L. Jiao, "Deep hash learning for remote sensing image retrieval," *IEEE Transactions on Geoscience and Remote Sensing*, vol. 59, no. 4, pp. 3420–3443, 2020. 9
- [51] C. Liu, J. Ma, X. Tang, X. Zhang, and L. Jiao, "Adversarial hash-code learning for remote sensing image retrieval," in *IGARSS 2019-2019 IEEE International Geoscience and Remote Sensing Symposium*. IEEE, 2019, pp. 4324–4327. 9
- [52] L. Yuan, T. Wang, X. Zhang, F. E. Tay, Z. Jie, W. Liu, and J. Feng, "Central similarity quantization for efficient image and video retrieval," in *Proceedings of the IEEE/CVF conference on computer vision and pattern recognition*, 2020, pp. 3083–3092. 9
- [53] Y. Cao, M. Long, B. Liu, and J. Wang, "Deep cauchy hashing for hamming space retrieval," in *Proceedings of the IEEE conference on computer vision and pattern recognition*, 2018, pp. 1229–1237. 9
- [54] S. Su, C. Zhang, K. Han, and Y. Tian, "Greedy hash: Towards fast optimization for accurate hash coding in cnn," *Advances in neural information processing systems*, vol. 31, 2018. 9
- [55] W.-J. Li, S. Wang, and W.-C. Kang, "Feature learning based deep supervised hashing with pairwise labels," *arXiv preprint arXiv:1511.03855*, 2015. 9
- [56] H. Zhu, M. Long, J. Wang, and Y. Cao, "Deep hashing network for efficient similarity retrieval," in *Proceedings of the AAAI conference on Artificial Intelligence*, vol. 30, no. 1, 2016. 9
- [57] Y. Yang and S. Newsam, "Bag-of-visual-words and spatial extensions for land-use classification," in *Proceedings of the 18th SIGSPATIAL international conference on advances in geographic information systems*, 2010, pp. 270–279. 7
- [58] G.-S. Xia, J. Hu, F. Hu, B. Shi, X. Bai, Y. Zhong, L. Zhang, and X. Lu, "Aid: A benchmark data set for performance evaluation of aerial scene classification," *IEEE Transactions on Geoscience and Remote Sensing*, vol. 55, no. 7, pp. 3965–3981, 2017. 7
- [59] G. Cheng, J. Han, and X. Lu, "Remote sensing image scene classification: Benchmark and state of the art," *Proceedings of the IEEE*, vol. 105, no. 10, pp. 1865–1883, 2017. 7
- [60] B. Thomee, D. A. Shamma, G. Friedland, B. Elizalde, K. Ni, D. Poland, D. Borth, and L.-J. Li, "Yfcc100m: The new data in multimedia research," *Communications of the ACM*, vol. 59, no. 2, pp. 64–73, 2016. 7
- [61] L. Van der Maaten and G. Hinton, "Visualizing data using t-sne." *Journal of machine learning research*, vol. 9, no. 11, 2008. 12, 13
- [62] R. R. Selvaraju, M. Cogswell, A. Das, R. Vedantam, D. Parikh, and D. Batra, "Grad-cam: Visual explanations from deep networks via gradient-based localization," in *Proceedings of the IEEE international conference on computer vision*, 2017, pp. 618–626. 13



Le Dong received the B.S. degree in n photogrammetry and remote sensing from Wuhan University, Wuhan, China, in 2016, and the Ph.D. degree in signal and information processing from the University of Chinese Academy of Sciences (UCAS), Beijing, China, in 2021. She is currently a assistant professor with the School of Artificial Intelligence, Xidian University. Her main research interests are hyperspectral image analysis, pattern recognition and machine learning.



Qixuan Cao received the B.S. degree in Intelligent Science and Technology, Shandong University of Science and Technology, Qingdao, China, in 2023. He is currently studying for a master's degree with the Institute of Artificial Intelligence in Xidian University. His research interests include deep learning, machine learning and image retrieval.



Lei Pu received the M.S. and Ph.D. degrees both from Air Force Engineering University, Xi'an, China, in 2016 and 2020, respectively. He has been a lecturer with the Combat Support College, Rocket Force Engineering University, Xi'an. His main research interests include visual tracking, pattern recognition, and computer vision.

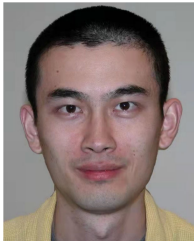


FangFang Wu received the B.S. degree in electronic engineering from the Xidian University, Xi'an, China, in 2008, and the Ph.D. degree in Intelligent Information Processing from Xidian University, Xi'an, China, in 2021. She is currently an assistant professor with the School of Artificial Intelligence, Xidian University. Her research interests include compressive sensing, Sparse representation, and deep learning.



Weisheng Dong (Member, IEEE) received the B.S. degree in electronic engineering from the Huazhong University of Science and Technology, Wuhan, China, in 2004, and the Ph.D. degree in circuits and system from Xidian University, Xi'an, China, in 2010. He was a Visiting Student with the Microsoft Research Asia, Beijing, China, in 2006. From 2009 to 2010, he was a Research Assistant with the Department of Computing, The Hong Kong Polytechnic University, Hong Kong. In 2010, he joined Xidian University as a Lecturer, where he has been a

Professor since 2016. He is currently with the School of Artificial Intelligence, Xidian University. His research interests include inverse problems in image processing, sparse signal representation, and image compression. He was a recipient of the Best Paper Award at the SPIE Visual Communication and Image Processing (VCIP) in 2010. He is also serving as an Associate Editor for IEEE TRANSACTIONS ON IMAGE PROCESSING and SIAM Journal on Imaging Sciences.



Xin Li (Fellow, IEEE) received the B.S. degree (Hons.) in electronic engineering and information science from the University of Science and Technology of China, Hefei, in 1996, and the Ph.D. degree in electrical engineering from Princeton University, Princeton, NJ, USA, in 2000. He was a member of Technical Staff with the Sharp Laboratories of America, Camas, WA, USA, from August 2000 to December 2002. Since January 2003, he has been a Faculty Member with the Lane Department of Computer Science and Electrical Engineering. In

2023, he joined the Department of Computer Science, University at Albany. He was elected as a fellow of IEEE in 2017, for his contributions to image interpolation, restoration, and compression.



Guangming Shi (Fellow, IEEE) received the B.S. degree in automatic control, the M.S. degree in computer control, and the Ph.D. degree in electronic information technology from Xidian University, Xi'an, China, in 1985, 1988, and 2002, respectively. He had studied at the University of Illinois and The University of Hong Kong. Since 2003, he has been a Professor with the School of Electronic Engineering, Xidian University, where he is currently the Academic Leader on circuits and systems. He has authored or coauthored over 200 papers in journals

and conferences. His research interests include compressed sensing, brain cognition theory, multirate filter banks, image denoising, low-bitrate image and video coding, and implementation of algorithms for intelligent signal processing. He was awarded the Cheung Kong Scholar Chair Professor by the Ministry of Education in 2012. He served as the Chair for the 90th MPEG and 50th JPEG of the International Standards Organization (ISO) and the Technical Program Chair for FSKD in 2006, VSPC in 2009, IEEE PCM in 2009, SPIE VCIP in 2010, and IEEE ISCAS in 2013.